catalysts

MDPI

Article

Photodeposition of Fe-Based Cocatalysts Capable of Effectively Promoting the Oxygen Evolution Activity of $BaTaO_2N$

Kanta Kobayashi [1], Takashi Hisatomi [2,3,*], Huihui Li [2,4] and Kazunari Domen [2,5,*]

[1] Department of Engineering, Graduate School of Science and Technology, Shinshu University, 4-17-1 Wakasato, Nagano-shi, Nagano 380-8553, Japan
[2] Research Initiative for Supra-Materials, Interdisciplinary Cluster for Cutting Edge Research, Shinshu University, Nagano-shi, Nagano 380-8553, Japan
[3] Precursory Research for Embryonic Science and Technology, Japan Science and Technology Agency, 4-17-1 Wakasato, Nagano-shi, Nagano 380-8553, Japan
[4] School of Materials and Energy, Lanzhou University, 222 South Tianshui Road, Lanzhou 730000, China
[5] Office of University Professors, The University of Tokyo, 2-11-16 Yayoi, Bunkyo-ku, Tokyo 113-8656, Japan
* Correspondence: hisatomi@shinshu-u.ac.jp (T.H.); domen@shinshu-u.ac.jp (K.D.)

Abstract: Activation of narrow bandgap photocatalysts is a prerequisite for the efficient production of renewable hydrogen from water using sunlight. Loading of dual cocatalysts intended to promote reduction and oxidation reactions by photodeposition is known to greatly enhance the water splitting activity of certain oxide photocatalysts. However, it is difficult to photodeposit oxygen evolution cocatalysts onto narrow bandgap oxynitride photocatalysts because the driving forces for the necessary oxidation reactions are weak. The present work demonstrates oxidative photodeposition of the Fe-based cocatalyst FeO_x onto a Mg-doped $BaTaO_2N$ photocatalyst having an absorption edge wavelength of 620 nm. This modification enhances the oxygen evolution activity of the photocatalyst more effectively than conventional impregnation methods. The rapid removal of photoexcited electrons from the photocatalyst by a reduction cocatalyst (Pt) and an electron acceptor (molecular oxygen) are evidently necessary for the photodeposition of the FeO_x cocatalyst. A Mg-doped $BaTaO_2N$ photocatalyst coloaded with Pt and FeO_x exhibits an apparent quantum yield of 1.2% at 420 nm during the oxygen evolution reaction in an aqueous $AgNO_3$ solution. This photodeposition procedure does not involve any heat treatment and so provides new opportunities for the design and construction of oxygen evolution sites on narrow-bandgap non-oxide photocatalysts that may be prone to thermal decomposition.

Keywords: oxynitride; visible light; water oxidation; coloading; electron removal

check for updates

Citation: Kobayashi, K.; Hisatomi, T.; Li, H.; Domen, K. Photodeposition of Fe-Based Cocatalysts Capable of Effectively Promoting the Oxygen Evolution Activity of $BaTaO_2N$. *Catalysts* **2023**, *13*, 373. https://doi.org/10.3390/catal13020373

Academic Editors: Eun Duck Park, Won Bae Kim and Ji-Wook Jang

Received: 16 December 2022
Revised: 23 January 2023
Accepted: 3 February 2023
Published: 8 February 2023

1. Introduction

Water splitting over particulate semiconductor photocatalysts has been studied as a means of generating renewable hydrogen from water using solar energy on a large scale [1]. However, the practicality of this process requires a solar-to-hydrogen energy conversion efficiency for photocatalytic water splitting of at least 5%. To meet this target, it will be necessary to develop narrow bandgap photocatalysts that can efficiently utilize visible light. Unfortunately, an oxide photocatalyst capable of splitting water into hydrogen and oxygen will typically have a bandgap equal to or greater than 3 eV, and so will not absorb visible light. This insufficient bandgap results from the valence band maximum, which is composed primarily of O 2*p* orbitals, being located at an overly positive potential (approximately +3 V vs. a reversible hydrogen electrode, or RHE) with respect to the oxygen evolution potential (+1.23 V vs. RHE) [2]. In contrast, certain transition metal-based semiconductor oxynitrides have a band gap narrow enough to absorb visible light while being highly chemically stable [3]. Furthermore, such materials have a bandgap suitable for water splitting into hydrogen and oxygen and have been reported to exhibit activity

during photocatalytic water splitting reactions based on one- and two-step excitation schemes [4,5]. In these materials, the valence band is mainly composed of hybridized O 2*p* and N 2*p* orbitals, while the conduction band primarily comprises *d* orbitals of the constituent transition metals. Because N 2*p* orbitals are located at more negative potentials than O 2*p* orbitals, the top of the valence band for an oxynitride will be shifted to a more negative potential compared with that for the corresponding oxide. The potential of the conduction band is not significantly affected, but the narrowed bandgap reduces the energy offset between the band-edge potential and the redox potential for the reactants, such that the driving force for the water splitting reaction is also reduced. It is, therefore, essential to load particulate oxynitride photocatalysts with cocatalysts to enhance their photocatalytic activity by promoting charge separation in the bulk material and to enhance surface redox reactions [6].

Here, $BaTaO_2N$ is a perovskite-type semiconducting oxynitride with a bandgap energy of 1.9 eV. This bandgap allows for the absorption of visible light at wavelengths up to 650 nm [7]. This material has been widely studied with regard to applications in photocatalytic water splitting systems and photoelectrochemical water oxidation reactions because it exhibits exceptional stability and has a bandgap that could permit overall water splitting and unassisted photoelectrochemical water oxidation under visible light [8–10]. Indeed, it has been experimentally confirmed that the bandgap straddles the redox potentials for hydrogen evolution and oxygen evolution reactions from water [11]. Recently, single-crystal $BaTaO_2N$ particles with low defect densities have been synthesized by a flux method [12]. When loaded with highly dispersed Pt nanoparticles serving as a reduction cocatalyst in such a way that there is intimate contact between the Pt nanoparticles and the photocatalyst, single-crystal particulate $BaTaO_2N$ has been shown to evolve hydrogen from an aqueous methanol solution with an apparent quantum yield (AQY) of 6.8% at a wavelength of 420 nm [13]. Furthermore, $BaTaO_2N$ can also evolve oxygen from an aqueous $AgNO_3$ solution with an AQY of 0.55% at 420 nm when loaded with cobalt oxide (CoO_x) as an oxygen evolution cocatalyst [14]. Doping of Mg into Ta sites in this compound has been reported to enhance the oxygen evolution activity of $BaTaO_2N$ by lowering the density of reduced Ta species, positively shifting the valence band edge [15]. A similar effect was observed by the present authors in a prior study [16]. Substitution of Ca for Ta was also reported to improve the oxygen evolution activity of the resultant $BaTaO_2N$ ($BaCa_{x/3}Ta_{1-x/3}O_{2+y}N_{1-y}$ ($0 \leq x, y \leq 1$)) [17]. However, the CoO_x was loaded by impregnation followed by heating at a high temperature under either an inert or reducing atmosphere. This process seemingly enhanced the n-type semiconducting properties of the $BaTaO_2N$ and, thus, decreased the hydrogen evolution activity of the material in our preliminary work. Consequently, it would be desirable to develop a means of loading oxygen evolution cocatalysts without the application of high temperatures.

Cobalt oxyhydroxide (CoOOH), intended for use as an oxygen evolution cocatalyst, has been loaded onto oxide photocatalysts, such as Al-doped $SrTiO_3$ and $BiVO_4$, by oxidative photodeposition, and has been found to enhance the oxygen evolution activities of these compounds [18,19]. This procedure does not involve heat treatment, but the oxidative photodeposition process requires the valence-band edge of the photocatalyst to be more positive than the redox potential of the cocatalyst ($CoOOH/Co^{2+}$ in the case of CoOOH). Therefore, it is difficult to effectively photodeposit CoOOH onto an oxynitride with a less positive valence-band edge, especially in the case of those compounds with absorption-edge wavelengths longer than 600 nm.

Among the various other oxygen evolution cocatalysts applicable to photocatalysts and photoanodes, iron oxyhydroxide (FeOOH) can be oxidatively deposited using Fe^{2+} ions at a relatively negative potential [20] and, thus, may be photodeposited onto narrow-bandgap materials, such as $BaTaO_2N$. In fact, FeOOH was previously photodeposited on an Al-doped $SrTiO_3$ photocatalyst and was found to promote the oxygen evolution activity of the photocatalyst [21].

In the present work, methods for the photodeposition of Fe-based cocatalysts (FeO_x) on particulate $BaTaO_2N$ and Mg-doped $BaTaO_2N$ ($BaTaO_2N$:Mg), and the subsequent effects on photocatalytic oxygen evolution activity, were investigated. The prompt removal of photoexcited electrons from these $BaTaO_2N$ photocatalysts was determined to be essential for the effective photodeposition of FeO_x cocatalysts and was also shown to improve the water oxidation activity.

2. Results and Discussion

The X-ray diffraction (XRD) patterns indicated that the major phase in both the $BaTaO_2N$ and $BaTaO_2N$:Mg samples was $BaTaO_2N$, which has a cubic perovskite structure (Figure S1) [22]. The $BaTaO_2N$:Mg was also found to contain small amounts of Ta_3N_5 [23] as a by-product, because the substitution of Mg for Ta generated an excess of Ta in the material [16]. The diffuse-reflectance spectroscopy (DRS) data showed that the onset of light absorption by the undoped and Mg-doped $BaTaO_2N$ occurred at approximately 660 and 620 nm, respectively (Figure S1). The substitution of Mg for Ta in these specimens would be expected to be accompanied by the replacement of N^{3-} by O^{2-} to maintain charge neutrality, thus, lowering the nitrogen content in the perovskite-type oxynitride. As a result, the top of the valence band should be shifted positively, and the bandgap should broaden. These effects were previously confirmed to occur in undoped and Mg-doped $BaTaO_2N$ by Zhang et al. using thermogravimetry and impedance spectroscopy [15]. The undoped $BaTaO_2N$ produced in the present work consisted of faceted particles several hundred nanometers in size with exposed smooth surfaces (Figure S1). It is also evident that doping with Mg both reduced the particle size and roughened the particle surfaces. Suppression of particle growth and formation of characteristic morphology by doping have often been observed in perovskite-type oxides, such as $NaTaO_3$ [24–26] and $SrTiO_3$ [27]. Compared with specimens fabricated in prior studies, the $BaTaO_2N$:Mg produced in this work exhibited stronger absorption at wavelengths longer than the absorption edge in addition to more distorted morphologies [16]. This could be ascribed to the deficiency of Ba species and to deviations from the desired temperature during the nitridation, because it was suppressed by adding additional Ba and adjusting the heating conditions. The effect of FeO_x photodeposition (as discussed below) was qualitatively reproducible regardless of variations in the $BaTaO_2N$:Mg products.

Figure 1 summarizes the initial oxygen evolution rates obtained using $BaTaO_2N$ and $BaTaO_2N$:Mg loaded with FeO_x and Pt cocatalysts under various conditions in aqueous $AgNO_3$ solutions. The undoped $BaTaO_2N$ showed a negligible oxygen evolution rate (<1 μmol h^{-1}), as did the specimen loaded with 0.1 wt% FeO_x by photodeposition. The material loaded with 0.1 wt% Pt by impregnation–reduction and that coloaded sequentially with and 0.1 wt% FeO_x by photodeposition were able to evolve oxygen, although the activity was still low. In contrast, the $BaTaO_2N$:Mg evolved oxygen at a higher rate even in the absence of the cocatalysts. This performance can possibly be ascribed to a positive shift in the valence band edge that resulted in a stronger driving force for holes involved in the oxygen evolution reaction [16]. Loading the photocatalyst with Pt by impregnation–reduction increased the oxygen evolution rate by a factor of approximately three, presumably because Pt promoted the extraction of photoexcited electrons from the photocatalyst [13]. Conversely, photodeposition of FeO_x alone did not appreciably affect the oxygen evolution rate. Notably, in the case that FeO_x was photodeposited after loading Pt by impregnation–reduction, the $BaTaO_2N$:Mg generated oxygen at a rate that exceeded the sum of the rates obtained for $BaTaO_2N$:Mg samples loaded with Pt by impregnation–reduction or FeO_x by photodeposition individually. This outcome was indicative of a synergistic effect obtained from coloading the Pt and FeO_x cocatalysts on the water oxidation activity of the $BaTaO_2N$:Mg.

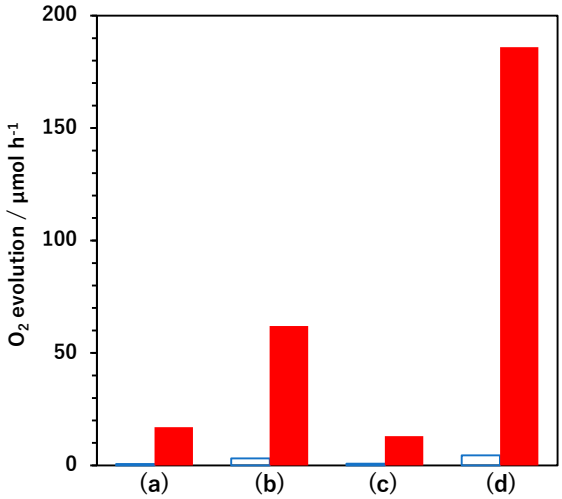

Figure 1. Oxygen evolution rates obtained from $BaTaO_2N$ (unfilled) and $BaTaO_2N$:Mg (filled) loaded with (**a**) no cocatalyst, (**b**) Pt (0.1 wt%) by impregnation–reduction, (**c**) FeO_x (0.1 wt%) by photodeposition, and (**d**) Pt (0.1 wt%) by impregnation–reduction followed by FeO_x (0.1 wt%) by photodeposition. Reaction conditions were as follows: photocatalyst, 0.2 g; distilled water, 120 mL; $AgNO_3$, 10 mM; La_2O_3, 0.1 g; 300 W Xe lamp (λ > 420 nm).

Oxygen evolution was found to cease when the $AgNO_3$ was depleted (Figure 2), confirming the stoichiometry of the sacrificial oxygen evolution reaction. Furthermore, there was a negligible production of nitrogen due to photo-oxidation of the oxynitride during these reactions. In the present system, the FeO_x species were evidently oxidatively photodeposited starting from Fe^{2+} ions and so the use of $FeCl_3$ instead of $FeCl_2$ as the Fe source did not enhance the oxygen evolution activity of the Pt-loaded $BaTaO_2N$:Mg (Figure 2). The Fe 2*p* X-ray photoelectron spectroscopy (XPS) analysis also suggested that the Fe species on the surface of the FeO_x species oxidatively photodeposited on the $BaTaO_2N$:Mg was not in the divalent state (Figure S2), because the binding energy of the Fe $2p_{3/2}$ orbital was evidently greater than 709.5 eV observed for $Fe_{0.94}O$ [28]. However, it was not possible to identify the chemical states of the Fe species conclusively using XPS because of the diversity of divalent and trivalent iron oxides and hydroxides. Moreover, it is considered that the FeO_x cocatalysts may have different chemical states during the water oxidation reaction (in water under illumination) and the XPS measurement (in vacuum under darkness). It is desirable to investigate the chemical states of Fe species by operando X-ray absorption spectroscopy [18] to reveal the working state of the FeO_x cocatalyst. Even so, based on prior research involving Al-doped $SrTiO_3$, it is assumed that the primary FeO_x species in these materials was FeOOH [21].

Even though the oxygen evolution rates were significantly different between the various specimens, inductively coupled plasma–optical emission spectroscopy (ICP-OES) analyses indicated that the amount of Fe photodeposited on the $BaTaO_2N$:Mg was essentially similar regardless of whether or not Pt was loaded. Specifically, the Fe concentrations were 0.30 and 0.34 wt% for the pristine material and 0.5 wt% Pt-loaded $BaTaO_2N$:Mg samples in the case that the nominal Fe loading was 0.5 wt%. This observation suggests that the Pt cocatalyst played a vital role by ensuring that the FeO_x cocatalyst was deposited in an effective state. It is likely that the Pt cocatalyst trapped photoexcited electrons and so promoted charge separation in the specimen that could have favored the photodeposition of FeO_x at oxidation sites on the $BaTaO_2N$:Mg. The importance of the rapid removal of photoexcited electrons during the photodeposition of FeO_x was also confirmed by studying the effect of molecular oxygen. That is, in the case that the photodeposition of FeO_x was conducted in the absence of molecular oxygen, the oxygen evolution activity of the Pt-loaded $BaTaO_2N$:Mg was only minimally enhanced (Figure 2). Likewise, in the absence of Pt, the photodeposition of FeO_x also did not improve the oxygen evolution activity

of the $BaTaO_2N$:Mg (Figure 1). These data suggest that molecular oxygen acted as an electron acceptor to promote the oxidative photodeposition of the FeO_x cocatalyst species. However, it should be noted that the photodeposition site of FeO_x was not controlled in the present samples unlike in the case of $SrTiO_3$:Al [21]. Figure 3 shows scanning electron microscope (SEM) images of the $BaTaO_2N$:Mg samples before and after loading 0.5 wt% Pt by impregnation–reduction and an additional 0.4 wt% FeO_x by photodeposition, where the cocatalyst loading was increased for the ease of observation. The Pt cocatalyst was mostly observed as nanoparticles smaller than 10 nm in size, although somewhat larger nanoparticles and aggregates also formed. After the subsequent photodeposition of FeO_x, additional nanoparticles and aggregates appeared to be deposited, often locally on some specific photocatalyst particles. However, it was difficult to identify the FeO_x cocatalyst or to distinguish the cocatalyst species. At least, the FeO_x cocatalyst did not appear to be photodeposited preferentially on oxidation sites of the $BaTaO_2N$:Mg particles, partly due to the non-uniform and distorted particle morphology. It is also probable that the flow of photoexcited charge carriers in $BaTaO_2N$:Mg was not well rectified due to defect levels characteristic of (oxy)nitride materials. Further refinement in the photocatalyst preparation will be required to define the loading sites and structures of FeO_x photodeposited on $BaTaO_2N$: Mg.

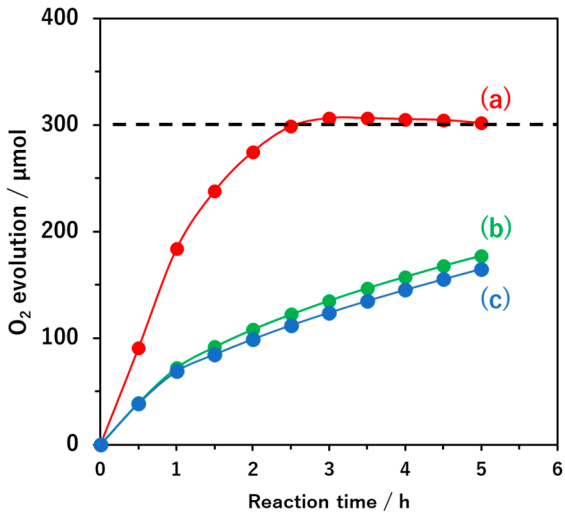

Figure 2. O_2 evolution from aqueous $AgNO_3$ solutions over time when using FeO_x/Pt/$BaTaO_2N$:Mg on which FeO_x was photodeposited (**a**) using $FeCl_2$ under ambient air, (**b**) using $FeCl_3$ under ambient air, and (**c**) using $FeCl_2$ in the absence of air. The horizontal black dashed line indicates the stoichiometric amount of O_2 that could be evolved from the amount of $AgNO_3$ added to the solution. Reaction conditions are as follows: $BaTaO_2N$:Mg, 0.2 g; Pt, 0.1 wt% loaded by impregnation–reduction; FeO_x, 0.1 wt% loaded by photodeposition; distilled water 120 mL; $AgNO_3$ 10 mM; La_2O_3 as a buffer 0.1 g; 300 W Xe lamp ($\lambda > 420$ nm).

Figure 4 presents a diagram showing a proposed mechanism by which the photodeposition of FeO_x promotes the oxygen evolution activity of $BaTaO_2N$:Mg. In this mechanism, in response to irradiation, electrons and holes are excited in the photocatalyst. The electrons are subsequently captured by the Pt cocatalyst and consumed in the oxygen reduction reaction in the presence of dissolved oxygen. Simultaneously, the holes oxidize Fe^{2+} ions in the solution to allow the oxidative deposition of FeO_x on the $BaTaO_2N$:Mg photocatalyst. In the absence of the Pt cocatalyst or molecular oxygen, the efficiency of charge separation will be lowered, which presumably prevents the photodeposition of FeO_x in active states on the $BaTaO_2N$:Mg. Further investigations will be required to establish the chemical states and structure of the FeO_x cocatalyst. Nevertheless, this is a rare example of an oxygen evolution cocatalyst photodeposited onto a narrow bandgap non-oxide photocatalyst that effectively promotes oxygen evolution activity. This process was enabled by loading Pt in

advance and providing molecular oxygen during the photodeposition process to ensure the rapid removal of photoexcited electrons. From Figure 1, it could be construed that doping with Mg induced a positive shift of the valence band edge that was a necessary perquisite for photodeposition of the FeO_x cocatalyst. However, the observed potential shift was as small as 0.1 eV, and so the impact of this shift on the photodeposition process is uncertain. Moreover, the oxygen evolution activity of undoped $BaTaO_2N$ coloaded with the Pt and FeO_x cocatalysts was enhanced to a greater extent when the oxynitride was re-nitrided for 1 h prior to cocatalyst loading. This observation suggests that Mg doping was not essential for effective FeO_x photodeposition but instead enhanced the intrinsic oxygen evolution activity of $BaTaO_2N$.

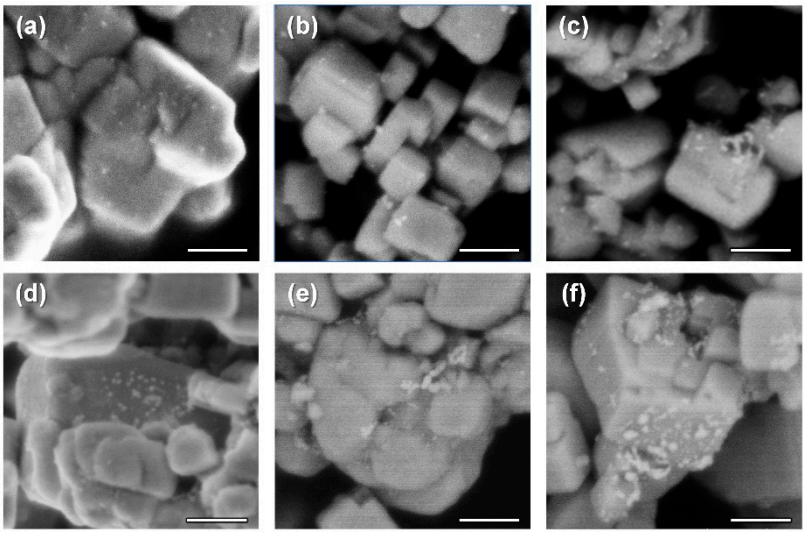

Figure 3. Secondary electron (**a**,**d**) and backscattered electron (**b**,**c**,**e**,**f**) SEM images of (**a**–**c**) Pt/$BaTaO_2N$: Mg and (**d**–**f**) FeO_x/Pt/$BaTaO_2N$: Mg. The loading amounts of Pt and FeO_x are 0.5 and 0.4 wt%, respectively. The scale bar is 100 nm.

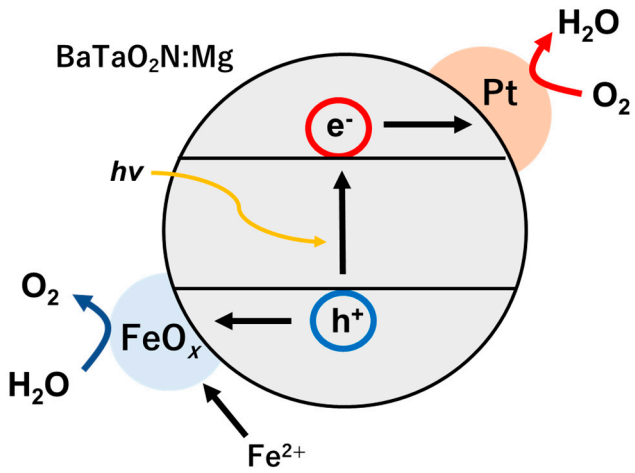

Figure 4. Diagram summarizing the oxidative photodeposition of FeO_x on Pt/$BaTaO_2N$:Mg.

To date, oxygen evolution cocatalysts have typically been loaded on oxynitride photocatalysts using impregnation methods and have been found to significantly improve oxygen evolution activity [14–17]. Therefore, in the present work, FeO_x cocatalysts were loaded on $BaTaO_2N$:Mg by impregnation followed by calcination under various conditions. Figure 5 compares the initial oxygen evolution rates over $BaTaO_2N$:Mg loaded with FeO_x cocatalysts using various processes from aqueous $AgNO_3$ solutions. The loading of FeO_x by impregnation followed by nitrogen annealing or hydrogen reduction and coloading of Pt and Fe by co-impregnation–hydrogen reduction enhanced the oxygen evolution activity of

$BaTaO_2N$:Mg. However, photodeposition of FeO_x following Pt loading was more effective. It is also important to stress that this photodeposition procedure did not require any heat treatment, unlike the impregnation methods. This new process is, therefore, expected to provide a practical approach to the coloading of hydrogen and oxygen evolution cocatalysts on thermally unstable non-oxide photocatalysts. In our previous work, one-step excitation overall water splitting was achieved by $BaTaO_2N$:Mg coloaded with Cr_2O_3-coated Rh as a hydrogen evolution cocatalyst and IrO_2 as a cocatalyst, where the former was loaded by impregnation–reduction and reductive photodeposition and the latter by adsorption [16]. It is expected that the FeO_x cocatalyst would be applicable as an oxygen evolution cocatalyst alternative to IrO_2. However, our preliminary trials were unsuccessful. The FeO_x cocatalyst appeared to degrade during the photodeposition of Cr_2O_3 in aqueous methanol solution. On the other hand, it seemed difficult to photodeposit FeO_x after Cr_2O_3 coating because the oxygen reduction reaction would be suppressed. To utilize the FeO_x cocatalyst effectively in the overall water splitting reaction, it is necessary to investigate the cocatalyst loading procedure carefully.

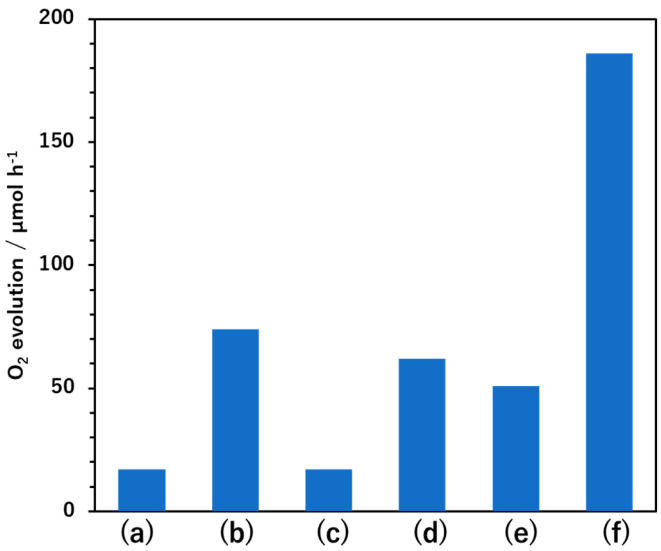

Figure 5. Oxygen evolution rates obtained for $BaTaO_2N$:Mg loaded with (**a**) no cocatalyst, (**b**) FeO_x by impregnation–nitrogen annealing, (**c**) FeO_x by impregnation–ammonia nitridation, (**d**) FeO_x by impregnation–hydrogen reduction, (**e**) FeO_x and Pt by co-impregnation–hydrogen reduction, and (**f**) Pt by impregnation–hydrogen reduction with subsequent FeO_x photodeposition. Reaction conditions were as follows: photocatalyst 0.2 g; distilled water 120 mL; $AgNO_3$ 10 mM; La_2O_3 as a buffer 0.1 g; 300 W Xe lamp (λ > 420 nm). The nominal Pt and Fe loadings were both 0.1 wt%.

Considering that the sequential coloading of Pt by impregnation–reduction and FeO_x by oxidative photodeposition promoted the oxygen evolution activity of $BaTaO_2N$:Mg, the FeO_x loading and the reaction conditions were optimized (Table 1). The oxygen evolution rate obtained from specimens in 10 mM $AgNO_3$ aqueous solutions was found to increase with an increasing FeO_x loading amount up to 0.2 wt%. However, the oxygen evolution was observed to decrease after the Ag^+ cations in the solution were rapidly consumed, and so the concentration of $AgNO_3$ was increased from 10 to 30 mM. At this higher concentration, the oxygen production rate plateaued at approximately 230 μmol h^{-1} for an FeO_x loading of 0.4 wt%. This FeO_x/Pt/$BaTaO_2N$:Mg sample exhibited an AQY of 1.2% at 420 nm during the oxygen evolution reaction. This value is lower than the AQY of 2.59% at 420 nm obtained for $BaTaO_2N$:Mg produced by nitridation of an amorphous oxide and loaded with CoO_x by impregnation–nitridation [15], but greater than that for $BaTaO_2N$ prepared by flux-assisted nitridation and loaded with CoO_x by impregnation–annealing (0.55% at 420 nm) [14]. Notably, nitridation of $BaTaO_2N$:Mg as a pretreatment prior to loading of the Pt and FeO_x cocatalysts was found to improve the oxygen evolution activity further. This

suggests that modifying the $BaTaO_2N$:Mg itself, such as by varying the degree of nitridation, crystallinity, or surface states, could also change the efficacy of the photodeposited FeO_x cocatalyst. Photodeposition of oxygen evolution cocatalysts is, therefore, a valid means of improving the $BaTaO_2N$ photocatalysts, and there is evidently much room for further improvement and for new applications.

Table 1. The O_2 evolution rates obtained for FeO_x/Pt/$BaTaO_2N$:Mg under visible light (λ > 420 nm) using various cocatalyst loading and reaction conditions.

Pretreatment of $BaTaO_2N$:Mg [a]	FeO_x Loading/wt% [b]	$AgNO_3$ Concentration /mM [c]	O_2 Evolution Rate /μmol h^{-1} [d]
No	0	10	44
No	0.05	10	110
No	0.1	10	186
No	0.2	10	196
No	0.2	30	143
No	0.4	30	231
Yes	0.4	30	385
No	0.8	30	232

[a] Nitrided for 1 h prior to the cocatalyst loading; [b] photodeposited from $FeCl_2$ in the presence of air after loading 0.1 wt% Pt by impregnation–reduction; [c] dissolved in distilled water containing 0.1 g of La_2O_3 as a pH buffer; [d] initial rate with 0.2 g of a photocatalyst specimen.

3. Experimental

3.1. Synthesis of Photocatalysts

Here, $BaTaO_2N$:Mg was employed as the primary photocatalyst in this work based on the positive shift of the valence band edge that could be achieved by doping [15]. Following our previous work [16], $BaCO_3$ (99.9%; Kanto Chemical Co., Inc., Tokyo, Japan), Ta_2O_5 (99.9%; High Purity Chemicals, Sakaido, Japan) and $Mg(NO_3)_2{\cdot}6H_2O$ (99.5%; FUJIFILM Wako Pure Chemical Corporation, Osaka, Japan) were combined in a Ba: Mg: Ta molar ratio of 1.1: 0.1: 1.0 and mixed in an agate mortar. Then, RbCl (95.0%; FUJIFILM Wako Pure Chemical Corporation, Osaka, Japan) was added as a flux at a Rb: Ta molar ratio of 9:1. The mixture was transferred to an alumina boat and heated at 1223–1253 K for 8 h under a flow of NH_3 (200 mL min^{-1}) in a tube furnace. After cooling to 303 K, the furnace was purged with N_2 and the product was removed, washed with distilled water, filtrated, and dried in air to obtain $BaTaO_2N$:Mg. In a representative case, a mixture of $BaCO_3$ (0.302 g), $Mg(NO_3)_2{\cdot}6H_2O$ (0.036 g), Ta_2O_5 (0.307 g), and RbCl (1.515 g) was nitrided. A sample of undoped $BaTaO_2N$ for comparison purposes was prepared in the same manner but without using the Mg source. In some cases, undoped and Mg-doped $BaTaO_2N$ were re-nitrided for 1 h without adding the RbCl flux as a pretreatment prior to loading of the cocatalyst.

3.2. Loading of Cocatalysts

Pt was loaded as a reduction cocatalyst using an impregnation method considering that the reduction activity of $BaTaO_2N$ was enhanced more effectively by loading Pt by impregnation than by photodeposition [13]. In this process, a portion of $BaTaO_2N$:Mg powder was suspended in an aqueous solution of $H_2PtCl_6{\cdot}6H_2O$ (98.5%; FUJIFILM Wako Pure Chemical Corporation, Osaka, Japan) in an evaporation dish. The amount of Pt was adjusted to give a concentration of 0.1 wt% with respect to the photocatalyst mass. The suspension was subsequently heated to dryness on a water bath while stirring with a glass rod. The resulting sample was then placed on an alumina boat and heated at 623 K for 1 h under a flow of 9 vol% H_2 + 91 vol% N_2 (220 mL min^{-1}) in a tube furnace. In a representative case, $BaTaO_2N$:Mg (0.21 g) was dispersed in a few milliliters of distilled water containing 132 μL of aqueous $H_2PtCl_6{\cdot}6H_2O$ solution (8.2 mmol L^{-1}) to give a Pt loading of 0.1 wt%. Subsequently, FeO_x was loaded as an oxygen evolution cocatalyst by photodeposition. A quantity of Pt-loaded $BaTaO_2N$:Mg powder was suspended in an aqueous solution (120 mL) of $FeCl_2{\cdot}4H_2O$ (99.0%; FUJIFILM Wako Pure Chemical Corpora-

tion, Osaka, Japan) and irradiated with visible light (λ > 420 nm) using a 300 W Xe lamp equipped with a cutoff filter for 1–5 h under air. In a representative case, Pt/$BaTaO_2N$:Mg (0.20 g) was dispersed in 120 mL of distilled water containing 40 μL of aqueous $FeCl_2.4H_2O$ solution (89.5 mmol L^{-1}) to give an Fe loading of 0.1 wt%. Note that, in other experiments, the photodeposition of FeO_x was conducted in the absence of air by connecting the reactor to a closed circulation system, evacuating the system, and introducing Ar to a pressure of 10 kPa. Some specimens were also produced using $FeCl_3{\cdot}6H_2O$ (99.9%; FUJIFILM Wako Pure Chemical Corporation, Osaka, Japan) as the Fe source. For comparison purposes, additional samples were generated using FeO_x loaded by an impregnation method. In these trials, the photocatalyst powder was suspended in an aqueous solution of $FeCl_2{\cdot}4H_2O$ in an evaporation dish and heated to dryness on a water bath while stirring with a glass rod. The resulting sample was placed on an alumina boat and heated for 1 h under a flow of 9 vol% H_2 + 91 vol% N_2 (220 mL min^{-1}), N_2 (200 mL min^{-1}) or NH_3 (200 mL min^{-1}) at 623, 1223, or 1023 K, respectively. Note that the FeO_x loading concentration is presented herein on the basis of elemental Fe regardless of the actual chemical state of Fe.

3.3. Photocatalytic Oxygen Evolution Reactions

Photocatalytic water oxidation reactions were carried out in a Pyrex top-illuminated reaction vessel connected to an airtight closed circulation system. In a typical procedure, a portion of FeO_x/Pt/$BaTaO_2N$:Mg (0.2 g) was dispersed in a 10 mM aqueous $AgNO_3$ solution (120 mL) containing La_2O_3 powder (0.1 g), in which the $AgNO_3$ functioned as a sacrificial electron acceptor and the La_2O_3 served as a pH buffer. The reaction solution was subsequently evacuated to remove dissolved air, after which Ar (10 kPa) was introduced into the closed circulation system and allowed to circulate until a homogenous gas phase was obtained inside the apparatus. The reaction was initiated by irradiating the sample with visible light ($420 \leq \lambda \leq 800$ nm) from above the reactor using a Xe lamp (LX-300F, INOTEX CO., LTD., Kamagaya, Japan) equipped with a cut-off filter (L42, HOYA, Tokyo, Japan) and a dichroic cold mirror. The reaction suspension was maintained at 288 K during irradiation using a cooling water circulator. The evolved gases were analyzed with a gas chromatograph (Shimadzu, GC-8A, Kyoto, Japan) equipped with molecular sieve 5A columns and a thermal conductivity detector, employing Ar (>99.999%) as the carrier gas.

3.4. Characterizations

The XRD patterns were acquired using a MiniFlex 300 powder diffractometer (Rigaku, Akishima, Japan) with Cu Kα radiation over the 2θ range of 10–80°. The UV–Vis DRS was conducted with a V-670 spectrophotometer (JASCO, Hachioji, Japan), using a Spectralon plate as a reference, over the wavelength range of 300–800 nm. Field-emission scanning electron microscopy (FE-SEM; SU-8000, Hitachi, Tokyo, Japan) was used to examine the morphologies of the photocatalyst samples. The XPS was performed using a PHI Quantera II spectrometer (ULVAC-PHI, Inc., Chigasaki, Japan) with an Al Kα radiation source. All binding energies were referenced to the C 1*s* peak (285.0 eV) arising from adventitious carbon. The amount of Fe loaded on each sample was determined by ICP-OES (ICPS-8100, Shimadzu, Kyoto, Japan). In preparation for this analysis, a photocatalyst sample (10 mg) was dissolved in a molten salt (2 g) comprising K_2CO_3 (99.5%, Kanto Chemical Co., Inc., Tokyo, Japan) and H_3BO_3 (99.5%, FUJIFILM Wako Pure Chemical Corporation, Osaka, Japan) combined at a 3:1 mass ratio. Following this, 10 mL of an aqueous solution of 5 wt% L(+)-tartaric acid prepared from commercial L(+)-tartaric acid (99.5%, FUJIFILM Wako Pure Chemical Corporation, Osaka, Japan), 4 mL of hydrochloric acid (1+1) made from commercial hydrochloric acid (35.0–37.0%, FUJIFILM Wako Pure Chemical Corporation, Osaka, Japan), 1 mL of an aqueous hydrogen peroxide solution (30.0–35.5 wt%, FUJIFILM Wako Pure Chemical Corporation, Osaka, Japan), and pure water were added to the molten salt mixture to obtain a total volume of 100 mL. This solution was diluted with pure water prior to the ICP-OES analysis when necessary.

The AQY value for each photocatalytic oxygen evolution reaction was calculated as follows:

$$\text{AQY (\%)} = [n \times R]/I \times 100$$

where n is the number of electrons consumed during oxygen production (with a value of 4), and R and I are the oxygen evolution rate and the number of incident photons per unit time, respectively. Each photocatalytic reaction was conducted under irradiation with a Xe lamp equipped with a bandpass filter with a peak wavelength of 420 nm. The light intensity at the sample surface was measured using a spectroradiometer (LS-100, EKO Instruments, Tokyo, Japan) to be 4.9×10^{20} photon h^{-1}.

4. Conclusions

Here, FeO_x was oxidatively photodeposited on Pt-loaded $BaTaO_2N$:Mg as a means of increasing the oxygen evolution activity of this photocatalyst. The rapid removal of photoexcited electrons from the photocatalyst was found to be essential for the effective photodeposition of FeO_x. Consequently, the presence of both Pt as a reduction cocatalyst and molecular oxygen as an electron acceptor during photodeposition was advantageous. The structure and chemical states of the photodeposited FeO_x species were not elucidated, but the FeO_x cocatalyst deposited in this manner was determined to be more effective than the same species loaded by impregnation followed by heat treatment. Assessment of the effects of the FeO_x loading amount and the reaction conditions allowed the optimized FeO_x/Pt/$BaTaO_2N$:Mg to exhibit an AQY of 1.2% at 420 nm during the oxygen evolution reaction in an aqueous $AgNO_3$ solution. Further performance improvements could likely be obtained by optimizing the FeO_x photodeposition conditions, and additional studies in this area could also provide a better understanding the nature of this cocatalyst. Importantly, the photodeposition procedure used in the present work did not involve any heat treatments. This is expected to lead to new opportunities for the design and construction of oxygen evolution sites on narrow-bandgap non-oxide photocatalysts that may be prone to thermal decomposition.

Supplementary Materials: The following supporting information can be downloaded at: https://www.mdpi.com/article/10.3390/catal13020373/s1, Figure S1: (A) XRD patterns, (B) DRS data, and (C) SEM images obtained for (a) $BaTaO_2N$ and (b) $BaTaO_2N$:Mg; Figure S2: Fe 2*p* XPS spectra of $BaTaO_2N$:Mg loaded with (a) no cocatalyst, (b) FeO_x by photodeposition, and (c) Pt by impregnation-hydrogen reduction with subsequent photodeposition of FeO_x.

Electronic Supplementary Information Available: Characterization of photocatalyst and cocatalyst samples.

Author Contributions: Conceptualization, T.H.; funding acquisition, T.H. and K.D.; investigation, K.K. and H.L.; project administration, T.H.; resources, T.H. and K.D.; supervision, T.H. and K.D.; validation, T.H.; writing—original draft, K.K.; writing—review and editing, T.H. and K.D. All authors have read and agreed to the published version of the manuscript.

Funding: This research was funded by JST, PRESTO, Japan (grant no. JPMJPR20T9), the Artificial Photosynthesis Project (ARPChem) of the New Energy and Industrial Technology Development Organization (NEDO, project no. P21021), the National Natural Science Foundation of China (grant no. 51402139), and the China Scholarship Council (grant no. 201906185004).

Data Availability Statement: The data presented in this study are available on reasonable request from the corresponding author.

Acknowledgments: The authors thank Michiko Obata and Ayaka Kikuchi of Shinshu University for assistance during the XPS analyses and SEM observations, respectively, and Keiko Kato of the University of Tokyo for assistance in the ICP-OES analyses.

Conflicts of Interest: The authors declare no conflict of interest.

References

1. Hisatomi, T.; Domen, K. Reaction systems for solar hydrogen production via water splitting with particulate semiconductor photocatalysts. *Nat. Catal.* **2019**, *2*, 387–399. [CrossRef]
2. Scaife, D.E. Oxide semiconductors in photoelectrochemical conversion of solar energy. *Sol. Energy* **1980**, *25*, 41–54. [CrossRef]
3. Jansen, M.; Letschert, H.P. Inorganic yellow-red pigments without toxic metals. *Nature* **2000**, *404*, 980–982. [CrossRef] [PubMed]
4. Wang, Q.; Domen, K. Particulate Photocatalysts for Light-Driven Water Splitting: Mechanisms, Challenges, and Design Strategies. *Chem. Rev.* **2020**, *120*, 919–985. [CrossRef] [PubMed]
5. Wang, Y.; Suzuki, H.; Xie, J.; Tomita, O.; Martin, D.J.; Higashi, M.; Kong, D.; Abe, R.; Tang, J. Mimicking Natural Photosynthesis: Solar to Renewable H_2 Fuel Synthesis by Z-Scheme Water Splitting Systems. *Chem. Rev.* **2018**, *118*, 5201–5241. [CrossRef] [PubMed]
6. Wang, Z.; Li, C.; Domen, K. Recent developments in heterogeneous photocatalysts for solar-driven overall water splitting. *Chem. Soc. Rev.* **2019**, *48*, 2109–2125. [CrossRef]
7. Kim, Y.; Woodward, P.M.; Baba-Kishi, K.Z.; Tai, C.W. Characterization of the Structural, Optical, and Dielectric Properties of Oxynitride Perovskites AMO_2N (A = Ba, Sr, Ca; M = Ta, Nb). *Chem. Mater.* **2004**, *16*, 1267–1276. [CrossRef]
8. Higashi, M.; Abe, R.; Takata, T.; Domen, K. Photocatalytic Overall Water Splitting under Visible Light Using $ATaO_2N$ (A = Ca, Sr, Ba) and WO_3 in a IO_3^-/I^- Shuttle Redox Mediated System. *Chem. Mater.* **2009**, *21*, 1543–1549. [CrossRef]
9. Higashi, M.; Domen, K.; Abe, R. Fabrication of an Efficient $BaTaO_2N$ Photoanode Harvesting a Wide Range of Visible Light for Water Splitting. *J. Am. Chem. Soc.* **2013**, *135*, 10238–10241. [CrossRef]
10. Higashi, M.; Yamanaka, Y.; Tomita, O.; Abe, R. Fabrication of cation-doped $BaTaO_2N$ photoanodes for efficient photoelectrochemical water splitting under visible light irradiation. *APL Mater.* **2015**, *3*, 104418. [CrossRef]
11. Balaz, S.; Porter, S.H.; Woodward, P.M.; Brillson, L.J. Electronic Structure of Tantalum Oxynitride Perovskite Photocatalysts. *Chem. Mater.* **2013**, *25*, 3337–3343. [CrossRef]
12. Luo, Y.; Wang, Z.; Suzuki, S.; Yubuta, K.; Kariya, N.; Hisatomi, T.; Domen, K.; Teshima, K. Fabrication of Single-Crystalline $BaTaO_2N$ from Chloride Fluxes for Photocatalytic H_2 Evolution under Visible Light. *Cryst. Growth Des.* **2020**, *20*, 255–261. [CrossRef]
13. Wang, Z.; Luo, Y.; Hisatomi, T.; Vequizo, J.J.M.; Suzuki, S.; Chen, S.; Nakabayashi, M.; Lin, L.; Pan, Z.; Kariya, N.; et al. Sequential cocatalyst decoration on $BaTaO_2N$ towards highly-active Z-scheme water splitting. *Nat. Commun.* **2021**, *12*, 1005. [CrossRef] [PubMed]
14. Okamoto, H.; Kodera, M.; Hisatomi, T.; Katayama, M.; Minegishi, T.; Domen, K. Effects of annealing conditions on the oxygen evolution activity of a $BaTaO_2N$ photocatalyst loaded with cobalt species. *Catal. Today* **2020**, *354*, 204–210. [CrossRef]
15. Zhang, H.; Wei, S.; Xu, X. Mg modified $BaTaO_2N$ as an efficient visible-light-active photocatalyst for water oxidation. *J. Catal.* **2020**, *383*, 135–143. [CrossRef]
16. Li, H.; Xiao, J.; Vequizo, J.J.M.; Hisatomi, T.; Nakabayashi, M.; Pan, Z.; Shibata, N.; Yamakata, A.; Takata, T.; Domen, K. One-Step Excitation Overall Water Splitting over a Modified Mg-Doped $BaTaO_2N$ Photocatalyst. *ACS Catal.* **2022**, *12*, 10179–10185. [CrossRef]
17. Wei, S.; Zhang, G.; Xu, X. Activating $BaTaO_2N$ by Ca modifications and cobalt oxide for visible light photocatalytic water oxidation reactions. *Appl. Catal. B* **2018**, *237*, 373–381. [CrossRef]
18. Lyu, H.; Hisatomi, T.; Goto, Y.; Yoshida, M.; Higashi, T.; Katayama, M.; Takata, T.; Minegishi, T.; Nishiyama, H.; Yamada, T.; et al. An Al-doped $SrTiO_3$ photocatalyst maintaining sunlight-driven overall water splitting activity for over 1000 h of constant illumination. *Chem. Sci.* **2019**, *10*, 3196–3201. [CrossRef] [PubMed]
19. Qi, Y.; Zhang, J.; Kong, Y.; Zhao, Y.; Chen, S.; Li, D.; Liu, W.; Chen, Y.; Xie, T.; Cui, J.; et al. Unraveling of cocatalysts photodeposited selectively on facets of $BiVO_4$ to boost solar water splitting. *Nat. Commun.* **2022**, *13*, 484. [CrossRef] [PubMed]
20. Beverskog, B.; Puigdomenech, I. Revised pourbaix diagrams for iron at 25–300 °C. *Corros. Sci.* **1996**, *38*, 2121–2135. [CrossRef]
21. Wang, S.; Teramura, K.; Hisatomi, T.; Domen, K.; Asakura, H.; Hosokawa, S.; Tanaka, T. Highly Selective Photocatalytic Conversion of Carbon Dioxide by Water over Al-$SrTiO_3$ Photocatalyst Modified with Silver–Metal Dual Cocatalysts. *ACS Sustain. Chem. Eng.* **2021**, *9*, 9327–9335. [CrossRef]
22. Pors, F.; Marchand, R.; Laurent, Y.; Bacher, P.; Roult, G. Etude structurale des perovskites oxyazotees $BaTaO_2N$ et $BaNbO_2N$: Structural study of $BaTaO_2N$ and $BaNbO_2N$ oxynitrided perovskites. *Mater. Res. Bull.* **1998**, *23*, 1447–1450. [CrossRef]
23. Brese, N.E.; O'Keeffe, M.; Rauch, P.; Disalvo, F.J. Structure of Ta_3N_5 at 16 K by Time-of-Flight Neutron Diffraction. *Acta Crystallogr. C Struct. Chem.* **1991**, *47*, 2291–2294. [CrossRef]
24. Kato, H.; Asakura, K.; Kudo, A. Highly Efficient Water Splitting into H_2 and O_2 over Lanthanum-Doped $NaTaO_3$ Photocatalysts with High Crystallinity and Surface Nanostructure. *J. Am. Chem. Soc.* **2003**, *125*, 3082–3089. [CrossRef]
25. Iwase, A.; Kato, H.; Kudo, A. The Effect of Alkaline Earth Metal Ion Dopants on Photocatalytic Water Splitting by $NaTaO_3$ Powder. *ChemSusChem* **2009**, *2*, 873–877. [CrossRef] [PubMed]
26. An, L.; Onishi, H. Electron−Hole Recombination Controlled by Metal Doping Sites in $NaTaO_3$ Photocatalysts. *ACS Catal.* **2015**, *5*, 3196–3206. [CrossRef]

27. Takata, T.; Jiang, J.; Sakata, Y.; Nakabayashi, M.; Shibata, N.; Nandal, V.; Seki, K.; Hisatomi, T.; Domen, K. Photocatalytic water splitting with a quantum efficiency of almost unity. *Nature* **2020**, *581*, 411–414. [CrossRef] [PubMed]
28. Yamashita, T.; Hayes, P. Analysis of XPS spectra of Fe^{2+} and Fe^{3+} ions in oxide materials. *Appl. Surf. Sci.* **2008**, *254*, 2441–2449. [CrossRef]